Substrate influence on two-dimensional solids and liquids: A Monte Carlo simulation study

Eduard Vives* and Per-Anker Lindgård
Physics Department, Risø National Laboratory, DK-4000 Roskilde, Denmark
(Received 19 July 1990)

A general model for two-dimensional solids and liquids on a substrate is studied by means of Monte Carlo simulation. The results can be applied to the case of adsorbed atoms or molecules on surfaces as well as intercalated compounds. We have focused on the study of the melting of a commensurate $\sqrt{3}\times\sqrt{3}$ structure on a triangular lattice with 1/3 coverage. The evolution of the energy, order parameters, and structure factor has been followed in a wide range of temperatures and substrate-potential strengths. The phase diagram exhibits a broad transition region between the solid and liquid phase for all the cases studied. We have in particular investigated the contribution from the two-dimensional liquid to the Bragg peaks corresponding to the substrate structure. Reiter and Moss and their collaborators have demonstrated that this gives valuable information about the substrate potential. A universal dependence is found between this and the particle fluctuations around the substrate potential wells. This dependence may be useful for an experimental determination of the magnitude of the substrate potential from scattering experiments, in particular for weak potentials and large atomic mean-square displacements.

I. INTRODUCTION

From a theoretical point of view, the problem of two-dimensional solids, liquids, and especially the melting transition is very interesting and has been studied intensively the last decades. A comprehensive review has been published recently.[1] It is known that a two-dimensional (2D) crystal does not have perfect long-range positional order, but instead exhibits a logarithmic decay of the positional correlations and only quasi-long-range order exists.[2] Kosterlitz and Thouless[3] demonstrated that although the true long-range positional order is not possible for a two-dimensional solid, it can exhibit a long-range orientational order of the particle bonds. This orientational order is destroyed by dislocations when the temperature is increased. Halperin, Nelson, and Young[4] completed the theory and showed that two consecutive continuous phase transitions may appear between the two-dimensional solid phase, with quasi-long-range positional order and true orientational order, and the liquid phase with no long-range order. The intermediate phase, so called hexatic phase, which exhibits quasi-long-range orientational order but no positional order has been under discussion during the last 20 years.[1] Experiments,[5–7] simulations,[8,9] and different theories[10] have been developed, sometimes with contradicting results.

A main reason for the prolonged discussion and lack of consensus is that real experiments are always performed on systems that are not perfectly two dimensional. Most of the experiments are performed with atoms physisorbed on substrates or intercalated between layers. We will focus our discussion on the adsorbed rare-gas atoms[11] and alkali metals intercalated in graphite.[12] Several factors are contributing to the difficulty in comparing these systems with the ideal two-dimensional solids and liquids. First of all there is the influence of the substrate potential, also called the corrugation potential. Depending on the competition between this interaction and the particle-particle interaction the solid phase at low temperature can be commensurate or incommensurate.[13] This fact is also important in the study of the melting of such systems. In general it is thought that the liquid and melting corresponding to incommensurate solids are less effected by the substrate potential.[14] Other factors are the motion of atoms perpendicular to the substrate,[15] the exchanges between the gas and the layer[16] in the adsorbed systems, and the influence between two consecutive intercalated layers[17] in the intercalated systems. Such effects will be neglected here. In this paper we focus on the substrate influence and limit the discussion to the case which has a commensurate solid phase at low temperatures. Our main aim is to perform a systematic study using Monte Carlo simulation, of the influence of the periodic substrate on the properties of two-dimensional solid and liquids, and to emphasize the observable effects on the structure factor, which can be measured in scattering experiments.

Two limiting cases have usually been discussed in order to characterize the substrate influence. The first assumes that the corrugation potential is large, so that the system can be considered as a lattice liquid in which the motion of the particles is restricted to a jumping between neighboring wells, while the motion within the substrate potential wells is not considered. In this limit several theories concerning modified Potts Models[18] have been developed, discussing mainly the symmetry change between the solid and liquid phase. Some of them[11] seem to be in agreement with the phase diagram for Kr adsorbed on graphite.[6] Very few calculations of the structure factors have been performed for these models, the only exception, to our knowledge, being the calculation of the structure factor of the lattice gas model using Monte Carlo simulation.[20] The second limit studied is based on the assumption that the substrate potential is relatively small and

can be considered as perturbing the real continuous liquid. A general theory, using both a perturbation and a cummulant expansion, of the substrate influence on the structure factor has been developed by Reiter and Moss[21] and has been proved do be successful in describing experiments on Rb (Refs. 22 and 23) as well as on K (Ref. 24) intercalated in graphite. The theory allow the possibility of extracting the corrugation potential from x-ray scattering data. The principal conclusion of the theory is that the 2D liquid produces an important contribution to the Bragg peaks of the substrate, and that the diffuse liquid ring structure factor may be reproduced around all the substrate peaks. In the absence of scattering from the substrate, the linear approximation of the theory predicts that the contribution to the Bragg peak intensity is proportional to $(V_{HK}/k_BT)^2$ where V_{HK} are the Fourier coefficients of the substrate potential, T is the thermodynamic temperature, and k_B is the Boltzmann factor. A quantitative comparison between these predictions and experiments is, however, not easy and therefore molecular dynamics calculations have been used[23,25] for tests. A main problem with this technique is that only relatively small systems can be studied within reasonable computer time, and finite-size effects may influence the results, in particular for a quantity like the structure factor. In this paper we propose instead a continuous Monte Carlo method, which allows the possibility of studying systems of 2700 atoms or more, thereby considerably reducing the finite-size effects.

A theory unifying the Potts lattice description and the continuous perturbed liquid description is needed in order to understand the influence of the substrate on the two-dimensional solids and liquids. Most experimental realizations seem to fall in a class between these limiting descriptions. We will focus on the calculations of the structure factor, because that can be directly compared with detailed scattering experiments. For this purpose it is particularily important to be able to study large systems, since the resolution of details in the structure factor are directly dependent on the spatial extent of the system. The structure factor offers a possibility for a measurement of the corrugation potential, the magnitude of which is under considerable discussion.[1]

The structure of the paper is as follows. In Sec. II we present our model and the main characteristics of the Monte Carlo simulation. In Sec. III the pair correlation functions and a number of order parameters are calculated. In Sec. IV we present the phase diagram for our model. In Sec. V the scattering properties are discussed and finally in Sec. VI we summarize and conclude.

II. THE MODEL

The model is defined on a 2D triangular reference lattice, with $L \times L$ sites i ($i=1,2,\ldots, N=L\times L$) and lattice parameter a. Each site in the lattice corresponds to the center of a hexagonal cell representing the substrate, see Fig. 1 with edge length $=a/\sqrt{3}$. Each cell can be occupied by only one atom. This particular symmetry has been chosen because it is the one corresponding to the (0,0,1) graphite surface ($a=2.456$ Å) which is the most

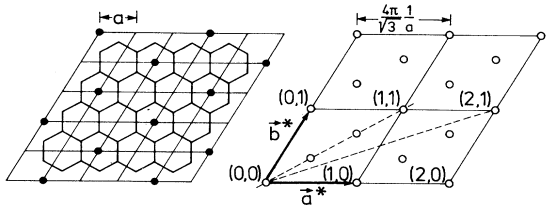

FIG. 1. Left, the direct reference lattice with the $\sqrt{3}\times\sqrt{3}$ structure indicated and the hexagonal cells. Right, the reciprocal space with the $\sqrt{3}\times\sqrt{3}$ Bragg peak positions indicated.

common substrate used for experiments on adsorbed atoms and intercalated compounds. The assumption of only one particle per cell is true for most of the adsorbates due to the large atomic (hard core) radius of the adatoms compared with the graphite lattice spacing.

On each site of the triangular lattice we define a variable S_i taking the two values 0 or 1 depending on the absence or presence of a particle at the cell i. Further we define $\mathbf{r}_i$ which is a 2D continuous vector that measures the position of the center of the atom inside the cell. We neglect the possibility of perpendicular motion of the particles. The total number of particles on the surface is kept constant so that

$$\sum_{i=1}^{N} S_i = cN \ , \tag{1}$$

where c is the coverage of the system. The Hamiltonian of the system is written as

$$H=\sum_{ij} S_iS_jV(|\mathbf{r}_i-\mathbf{r}_j-\mathbf{R}_{ij}|)+\sum_{i=j}^{N} S_iU(|\mathbf{r}_i|) \ , \tag{2}$$

where the first term represents an isotropic interaction between the particles and the second term the particle substrate corrugation interaction, assumed to be isotropic around each cell center. The first summation is a sum over all pairs of sites in the lattice and the second summation is a single sum over the lattice sites. $\mathbf{R}_{ij}$ represents the vector joining cell centers at sites i and j.

It is known that in real systems, in particular for metal surfaces, the interactions are more complicated, usually exhibiting anisotropic particle-particle interactions due to the electronic exchange with the substrate and a breakdown of the pair interaction assumption,[14] etc. Such effects could be included but are neglected for simplicity.

The Hamiltonian allows the possibility of clearly identifying the two limits described in the Introduction. On the one hand, when the corrugation potential U is very big, the only effect of the second term is to force the particles to occupy the cell centers and restrict the possible movement to jumps between the sites. The system is then described by the S_i variables only. On the other hand, in the case of no substrate effect, the S_i variables are irrelevant and the first summation is a sum over particles interacting through an isotropic potential. The intermediate case, as demonstrated by Fan *et al.*,[25] does exhibit interesting coupling phenomena between the $\mathbf{r}_i$ and

S_i variables in the same way as in other Hamiltonians used for the description of coupled phase transitions.[26]

Although the formulation of the model is general, we have focused on a simple case with $U(r)$ being a parabolic potential and $V(r)$ being a Lennard-Jones[27] like interaction. $U(r)$ is defined in such a way that it takes a zero value at the corners of the hexagonal cell and $-\varepsilon U (U>0)$ at the center of the cell, where ε is an energy unit:

$$U(r)=-\varepsilon U[1-3(r/a)^2] . \tag{3}$$

In order to compare with the results of Reiter and Moss[21] we have calculated the first few Fourier expansion coefficients for this potential

$$U(x,y)=\varepsilon U \sum_{H,K} V_{HK} \exp\left[2\pi i\left[\frac{x}{a}\frac{K}{\sqrt{3}}+\frac{y}{a}\frac{K+2H}{\sqrt{3}}\right]\right] , \tag{4}$$

where H,K are integer numbers indexing the sites in the reciprocal lattice. The first coefficients are

$$V_{0,0}=0.583\,292\,64 ,$$

$$V_{1,0}=V_{0,1}=V_{-1,1}$$
$$=V_{-1,0}=V_{0,-1}=V_{1,-1}=-0.094\,289\,79 ,$$

$$V_{1,1}=V_{2,-1}=V_{1,-2}$$
$$=V_{-1,-1}=V_{-2,1}=V_{-1,2}=0.025\,408\,26 .$$

Note that the first coefficient of the corrugation potential is in this case only -9.4% of εU.

The Lennard-Jones potential has been extensively used for the study of the rare-gas atomic interaction. It is defined as

$$V_{LJ}(r)=4\varepsilon\left[\left[\frac{\sigma a}{r}\right]^{12}-\left[\frac{\sigma a}{r}\right]^{6}\right] . \tag{5}$$

Here ε is the energy scale of the Lennard-Jones potential. All energies will be given in units of ε and the temperatures as $T=k_BT/\varepsilon$. The depth of the attractive well is ε and σa is proportional to the position of the potential minimum ($r_{\min}=2^{1/6}\sigma a$) for $V_{LJ}(r)$.

In order to reduce the computer time, we introduce two cuts in the Lennard-Jones potential:

$$V(r)=\begin{cases}\infty & \text{if } r<r_1\\ V_{LJ}(r) & \text{for } r_1<r<r_2\\ 0 & \text{if } r>r_2 .\end{cases} \tag{6}$$

Here r_1 is chosen to prevent particles from occupying the same cell by assuming that the interaction energy of two particles is infinite if they are in the same cell. This gives $r_1=2a/\sqrt{3}$, i.e., the maximum distance between two points inside of a cell. The distance r_2 is chosen so that the interaction is zero when they are separated more than the sixth neighbor cell, giving $r_2=4a/\sqrt{3}$, i.e., the minimum distance between two sixth neighbors cells, see Fig. 1. With these definitions the first summation over lattice pairs in (2) can be performed including the fifth neighbors without loosing the isotropy of the potential. A further restriction of the summation over the pairs in (2) without reducing the potential cut r_2 will lead to an anisotropy in the system even in the case $U=0$. With our choice we maintain the complete isotropy of the liquid also in the limit $U=0$. Therefore the influence of the reference lattice vanishes when the corrugation disappears. Let us define the Hamiltonian H_0 for the cut potential and that for the tail ΔH, giving $H=H_0+\Delta H$.

In this paper we study the commensurate case with $2^{1/6}\sigma=\sqrt{3}$ and $c=\frac{1}{3}$, so that the minimum of the particle-particle interaction is exactly at the second neighbor distance on the substrate lattice. With these definitions the ground state of the system is a commensurate structure (usually called a $\sqrt{3}\times\sqrt{3}$ structure) with degeneracy 3 in the case of $U>0$. For $U=0$ the system has continuous translation and rotational symmetry.

The simulation of this system is performed using standard Monte Carlo techniques.[28] We use a 90×90 triangular lattice with periodic boundary conditions in order to minimize the boundary effects. This represents a lattice with 8100 sites and 2700 particles when $c=\frac{1}{3}$. The position of the molecules is updated sequentially on the lattice, and the proposed position is obtained performing uniformly distributed random steps inside of a circle of radius r_d around the old position. When the proposed position is outside of the original cell, the change is considered as an attempt to jump to a new cell, and if the movement is accepted the variables S_i are updated. By this method we assure that the particle diffusion is isotropic for $U=0$, which has been tested. The size of r_d will determine the speed of the Monte Carlo simulation. We have chosen $r_d=0.2a$ which gives an acceptation ratio of 0.5 in a large range of intermediate temperatures. Considering that we are not particularly interested in the dynamics of the system, but in the equilibrium properties, this value is quite good.

The averages of the interesting quantities are taken over 3000–6000 MCS (1 MCS = 1 Monte Carlo step = 1 attempt per particle) after discarding the first 4000–8000 MCS's in order to equilibrate the system. Averages over different runs, using different random number generator seeds, are also taken in order to improve the statistics of the results.

III. THE PAIR CORRELATION FUNCTION $g(r)$ AND ENERGY $E(T)$ AT $U=0$

In order to reach firm conclusions about the effects of the corrugation potential U, it is important to test the liquid structure for $U=0$. Firstly, that the structure is not influenced by the underlying reference lattice and secondly that no unphysical features are introduced by the truncated Lennard-Jones potential. Figure 2 shows the structure at "full coverage" $c=\frac{1}{3}$ obtained after melting a perfect $\sqrt{3}\times\sqrt{3}$ structure on the reference lattice and letting it reach equilibrium in 7000 MCS. It is isotropic with no obvious signs of memory of the orientation of the initial ordered structure. Both pictures show the

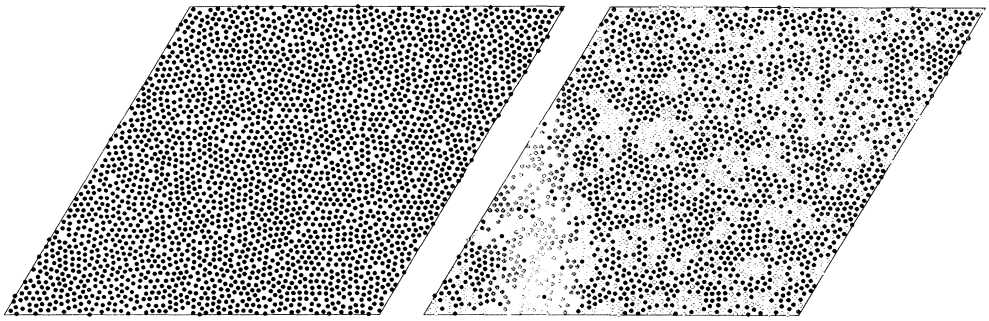

FIG. 2. Left, snapshot of the simulated liquid phase. Right, same with particles with different number of neighbors n indicated ● $n>6$, ⊗ $n=6$, and ○ $n<6$.

same structure, but to the right an analysis is made showing the number of neighbors each particle has. It is evident that the liquid has a fluctuating density with open areas and denser crystallinelike patches of various orientations. The pair correlation, averaged over direction, $g(r)$ is calculated directly including r up to $13a$. As expected for high coverages, there is no sign in $g(r)$ of the truncation of the potential V_{LJ} at $r=4a/\sqrt{3}$. Assuming *a priori* that $g(r)$ is correct, we can calculate the effect of the truncation on the internal energy per particle E and the free energy at high T. Using $F=-T\ln Z$ with $Z=\mathrm{Tr}\{\exp[-(H_0+\Delta H)/T]\}$ and expanding to first order in $\Delta H/T$ one obtains

$$F_{LJ}=F_0-\langle \Delta H\rangle_0+o(1/T)\ , \tag{7}$$

where the index 0 indicates properties obtained in the Monte Carlo simulation with the truncated $V_{LJ}(r)$ potential. The main effect of the cut is a correction to the internal energy per particle. Equation (7) is valid also at $T\to 0$. The calculated $E(T)$ is shown in Fig. 3, and it is demonstrated that the energy, corrected for the neglected contribution from the tail according to (7) using the calculated $g(r)$, agrees excellently with that obtained by Abraham.[27] Figure 4(a) shows furthermore that our $g(r)$ for the liquid agrees in all details with that obtained by Abraham[27] and so does that for the solid, Fig. 4(b).

We conclude that our Monte Carlo scheme gives results in good agreement with previous calculations and shows no anisotropy for $U=0$.

IV. PHASE DIAGRAM AS A FUNCTION OF U

In the following we study mainly the case of coverage $c=\frac{1}{3}$ with variable corrugation potential and with the LJ potential favoring the $\sqrt{3}\times\sqrt{3}$ structure with the same lattice constant, i.e., with $\sigma=3^{1/2}2^{-1/6}$. For all U studied we find a transition region. Because the pressure is increasing rapidly in this region, it most probably can be characterized as a mixed phase region. It is not the purpose of this paper to discuss a possible hexatic phase region. For very large U the model reduces to a 3-state Potts model for which it is known that the transition is a single continuous one. We have not aimed at studying sufficiently high U to observe this. The phase diagram was obtained by starting from a single domain $\sqrt{3}\times\sqrt{3}$ structure and also by cooling from the liquid phase. In the latter case one reaches a (probably) metastable multidomain structure shown in Fig. 5 for $U=0$, $T=0.1$ and $c=0.323\,33$. It has clearly no preferred orientation of the crystallites. To the right is seen an analysis showing that particles with 5 and 7 neighbors are concentrated along the grain boundaries. We return to a more detailed discussion of the possibility that this is a Kosterlitz-Thouless phase and of a possible hexatic phase elsewhere.

The following several parameters were monitored in order to display the transition.

(a) The change in slopes of $E(T)$, see Fig. 3.

(b) We have studied a number of local order parameters. Figure 6(a) shows the temperature dependence of the average $\langle|\Psi|^2\rangle$ and $|\langle\Psi\rangle|^2$ of the local orientational nearest-neighbor parameter defined on each occupied cell as

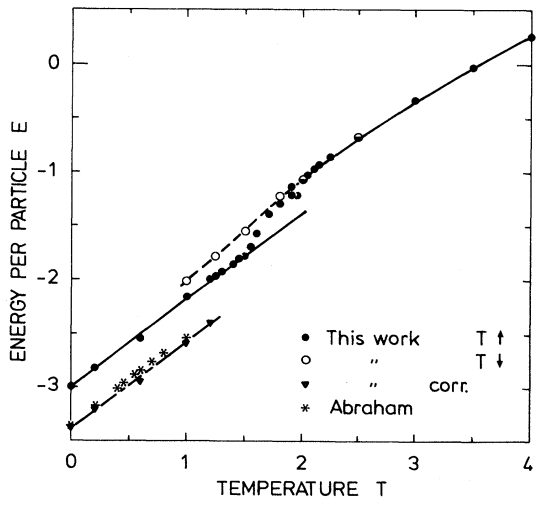

FIG. 3. The energy per particle as a function of temperature. The energy (▼) corrected for the effects of the cutoff $\langle\Delta H\rangle_0$ agrees well with that obtained by Abraham (Ref. 8).

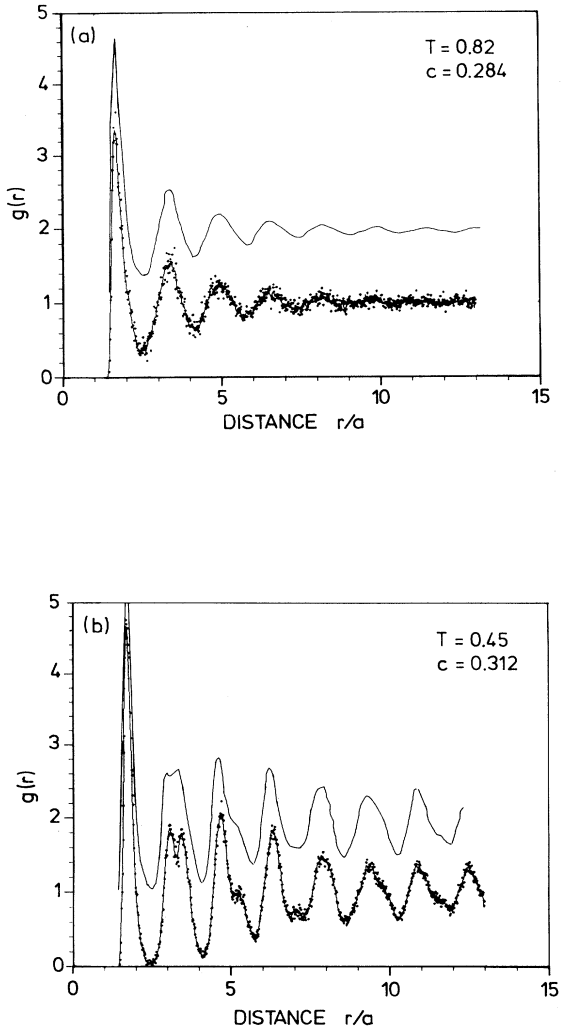

FIG. 4. (a) The paircorrelation function $g(r)$ for the liquid phase compared with Abrahams (Ref. 16) $g(r)+1$, thin line. (b) Same for the solid phase.

$$\Psi(\mathbf{r}_i)=\frac{1}{6}\sum_{p=1}^{n_i} e^{i6\theta_{ip}} , \tag{8}$$

where the sum over p runs over the number of interacting neighbors n_i at site i, and θ_{ip} is the bond angle with respect to a reference axis. These parameters again show clear anomalies (upon heating) at $T\sim 2$ for $U=0$. In Fig. 6(b) is shown the positional particle fluctuation parameter $\langle u^2\rangle=\langle r^2\rangle-\langle r\rangle^2$ around the ordered structure position, i.e., the reference lattice site. The parameter $\langle u^2\rangle$ has an anomaly at the low temperature side of the transition region, again consistent with the anomaly in $E(T)$ at $T\sim 1.55$ for $U=0$. At higher temperatures it goes to the value 5/36, which is the theoretical value calculated assuming a random distribution of the particles inside the hexagonal cells. We have also considered another, extrapolated definition of the positional fluctuations $\langle u^2\rangle_e$ by fitting the distribution of particles inside the cells to a Gaussian distribution of the form

$$Ae^{-r^2/\langle u^2\rangle_e} . \tag{9}$$

We have found that $\langle u^2\rangle_e$ diverges at $T\sim 1.55$ for $U=0$. This is physically reasonable, and we preferentially use this definition in the following analyses.

(c) We also followed the long-range decrease of $g(r)$ and that of the orientational order parameter $g_6(r)$ defined as

$$g_6(r)=\langle \Psi(0)\Psi^*(r)\rangle . \tag{10}$$

The available large-r behavior was not found to be exponential, but is better described as an algebraic decay of the form

$$g(r)-1\sim r^{-\eta} , \quad g_6(r)/g(r)\sim r^{-\eta_6} . \tag{11}$$

This is demonstrated in Fig. 7(b) together with the temperature dependence of the exponents, Fig. 7(a). Possibly, we are not able to measure the decay at sufficiently large r to obtain an exponential decay, as expected from theory.[4] Here we are primarily using the variation of the

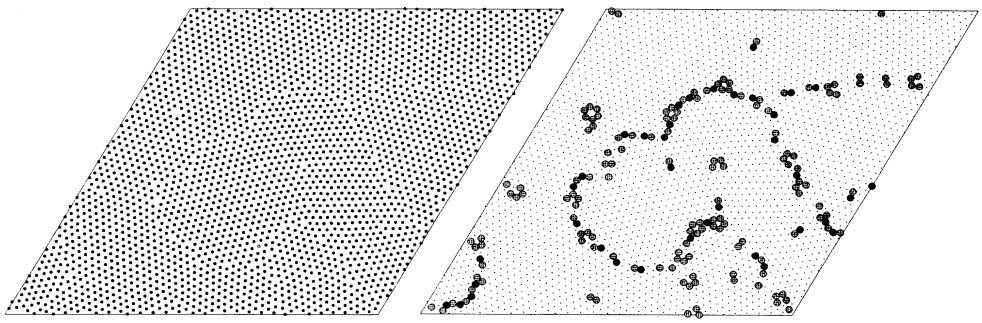

FIG. 5. Left, the solid formed after a quench of a high-T liquid after 2000 MCS, $c=0.3233$, $T=0.1$. Randomly oriented domains are formed. Right, same with particles having 5 and 7 neighbors indicated by ⊗ and ●, respectively. Grain boundaries with pairs of 5–7 and defects are clearly visible.

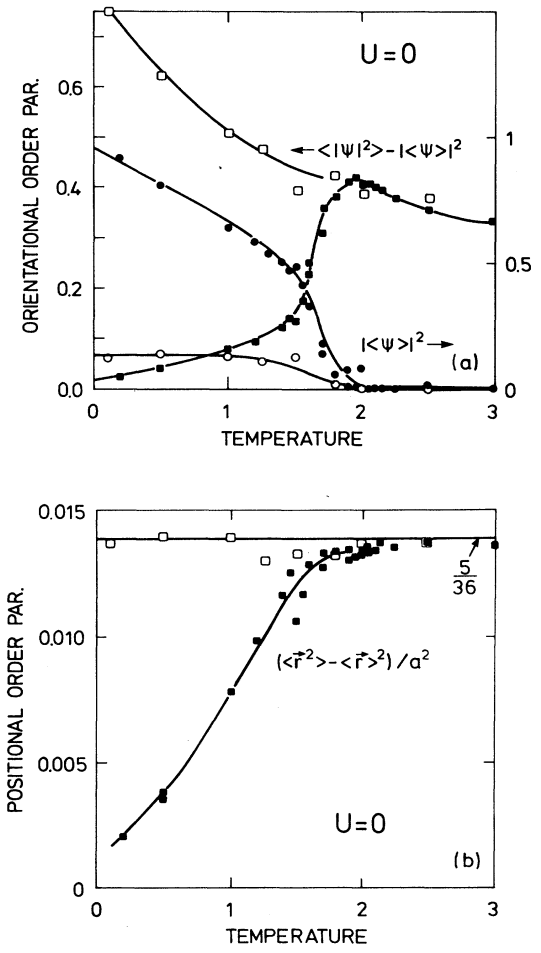

FIG. 6. (a) The local orientational order parameters $\langle|\Psi|^2\rangle-|\langle\Psi\rangle|^2$ (square) and $|\langle\Psi\rangle|^2$ (circle) as a function of T for $U=0$. The arrows point toward the relevant axes. Clear anomalies occur at $T\sim 2$. Black signatures represent results for heating from a perfect $\sqrt{3}\times\sqrt{3}$ structure and open signatures for cooling from the liquid phase. It shows that crystal growth and melting is irreversible. (b) The positional fluctuation parameter $(\langle r^2\rangle-\langle r\rangle^2)/a^2$ showing an anomaly at $T\sim 1.55$ close to the low-T side of the transition region. The exact high-T limit 5/36 is reproduced, thin line. Notice that upon cooling of the liquid (open symbols), the formed solid has no correlation with the reference lattice.

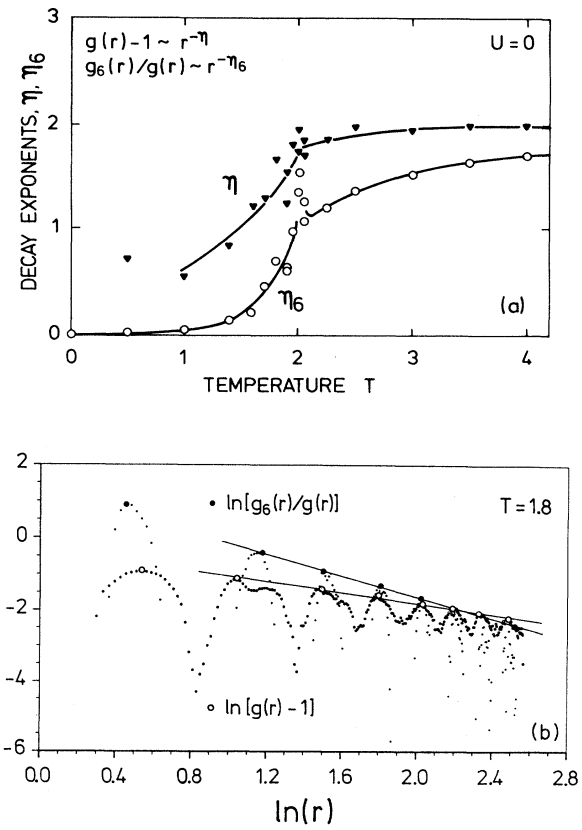

FIG. 7 (a) Decay exponents η and η_6 for the simple and the orientational pair correlation functions $g(r)-1$ and $g_6(r)/g(r)$. Clear anomalies occur at $T=2$ for $U=0$. (b) Plot of the logarithm of the correlation functions $g_6(r)/g(r)$ and $g(r)-1$. It demonstrates that the decay is algebraic and not exponential as anticipated by Halperin and Nelson (Ref. 4). The symbols ○ and ● indicate the maximum of $\ln[g_6(r)/g(r)]$ and $\ln[g(r)-1]$, respectively, and the thin lines are guides to the eye.

long-range behavior of the correlation functions as an indicator for the melting transition. We have found that both exponents show a clear anomaly at $T=2$ for $U=0$ consistently with the change in $E(T)$.

The phase diagram obtained in this way is shown in Fig. 8. Scans performed by varying T or U are indicated with heavy lines, the dots indicate that the lower phase boundary is rather more difficult to define accurately. As expected the transition temperature rises at first linearly with increasing corrugation potential. This study is the first of the melting transition at coverage $c=\frac{1}{3}$. It is in qualitative agreement with that of Barker *et al.*[29] for variable coverage $c<\frac{1}{3}$.

V. SCATTERING PROPERTIES

The main purpose of this paper is to discuss the behavior of the static structure factor $S(\mathbf{q})$, which can be measured in an x-ray or neutron-scattering experiment. The structure factor is calculated as discussed in Appendix A and defined as

$$S(\mathbf{q})\equiv\frac{1}{N_p^2}\left\langle\left|\sum_{i=1}^{N_p}e^{i\mathbf{q}\cdot\mathbf{r}_i}\right|^2\right\rangle, \tag{12}$$

where $N_p=N/3$ is the number of particles. It is normalized to 1 for $q=0$ and approaches $1/N_p$ for $q\to\infty$. In the liquid phase the structure factor can be well fitted by a sum of Lorentzians and a slightly sloping, flat background as can be seen in Fig. 9. However, some small discrepancies are systematically present. Figure 10(a)

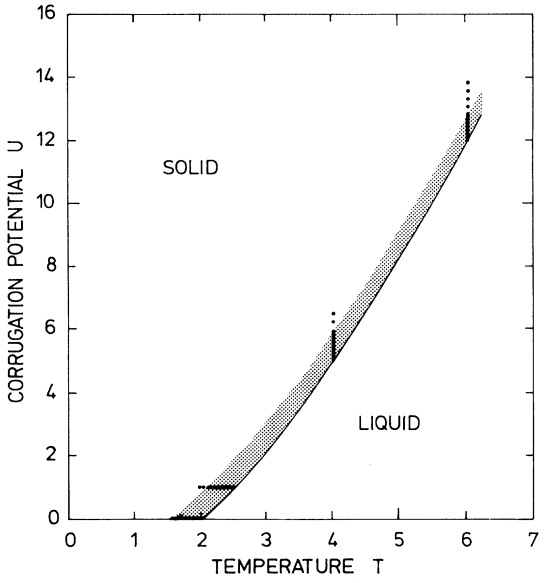

FIG. 8. The phase diagram for coverage $c=\frac{1}{3}$ as a function of temperature and corrugation potential U. The shaded area indicates the transition region obtained from the indicated scans.

shows the evolution of $S(\mathbf{q})$ as a function of temperature for $U=0$. We follow three $\mathbf{q}$ vectors, see Fig. 1(b). The column indexed by $q(11)$ shows the results for the $\mathbf{q}$ vector which contains the Bragg peaks at $\mathbf{q}=(1,1)q_0/3$ and $(1,1)2q_0/3$ of the (chosen) ordered $\sqrt{3}\times\sqrt{3}$ structure of the reference lattice, $q_0=4\pi/(\sqrt{3}a)$ is the wave-vector unit, see Fig. 1. The $q(21)$ column shows a low symmetry direction and the $q(10)$ column the direction which contains the Bragg peak at $\mathbf{q}=(1,0)q_0$ of a possible substrate together with a $\sqrt{3}\times\sqrt{3}$ Brag peak from the surface layer with the reference lattice structure. The $q(11)$ sequence shows clearly the transformation of the large

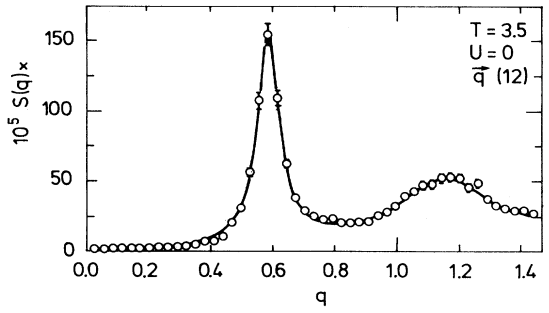

FIG. 9. A typical structure factor $S(\mathbf{q})$ for $\mathbf{q}=(1,2)q_0$. The thin line represents a fit to two Lorentzians and a slightly sloping background. From this the peak position is extracted. As discussed in Appendix A the density q point is higher in the other $\mathbf{q}$ directions.

low temperature Bragg peaks. They have no width at $T=0$, but have developed "feet" at $T=0.5$. At the upper transition temperature $T=2$ these "feet" become the liquid diffuse scattering $S^l(\mathbf{q})$. The structure in the $q(21)S(\mathbf{q})$ at low T is due to the influence of the "feet" from the neighboring Bragg points. This is evident from Fig. 1. It is not a signature of liquid ring structure in the solid phase. At high temperature $T=4$ the diffuse scattering forms an isotropic ring as demonstrated by the three cuts $q(11)$, $q(21)$, and $q(10)$. Close to the melting point there is indication of some modulation of the ring (different from that expected for the initial lattice orientation). This feature needs further study. It probably disappears if an average is taken over many different runs.

Figure 10(b) shows that a very similar behavior, at first sight, is obtained by varying the corrugation potential. An important difference is the modulation of the ring in the liquid phase, which for $U<4.5$, shows a clear memory of the orientation of the underlaying lattice. This is as expected. Another very important feature is the persistence of the Bragg peak at $\mathbf{q}=(1,0)q_0$. This is the strongest sign of a lattice modulated liquid. In our simulation we, of course, do not see the substrate Bragg peak, but only the contribution from the surface layer. At the studied potential values no clear sign of peaks from possible secondary liquid rings around the (10) Bragg peaks are visible. A third important feature evident from the series of $S(\mathbf{q})$ in Fig. 10 is that there is no shift in the peak position of the first peak near the melting point. An accurate peak position was determined by Lorentzian fits as shown in Fig. 9. It must be remembered that we are studying the case of constant coverage and therefore a variable pressure. At constant pressure the position of the first peak may well move to smaller q values in the liquid phase. It is therefore quite difficult to interpret a possible experimentally observed shift of the peak position, in particular as a sign of a hexatic phase. The induced contribution to the substrate Bragg peak $S(\mathbf{q}_{10})$ has a number of intersting features. The peak intensity of $S(\mathbf{q}_{10})$ is shown in Fig. 11(a) as a function of temperature for $U=1$ and in Fig. 11(b) as a function of decreasing corrugation potential. It shows a clear anomaly in the transition region (close to the low T side) and in the liquid phase. The logarithm of the intensity decreases linearly toward the diffuse scattering of the liquid $S(\mathbf{q}_{10})\rightarrow 1/N_p=0.000\,37$ for high T. The behavior as a function of decreasing corrugation potential Fig. 11(b) is qualitatively similar. In the Reiter and Moss linear theory[21] the intensity of the induced Bragg peak is solely dependent on the ratio (U/T), squared. The thin lines, Figs. 11(a) and 11(b), are calculated using the first Fourier component Eq. (4). Since the expansion parameter for the theory is then approximately only $-\frac{1}{10}$ of (U/T), the linear theory could be expected to apply to all our studied values of U and T in the liquid region. The fit is excellent for relatively large U and T, Fig. 11(b). However, for small U the Bragg peak intensity obtained in the MC simulation starts larger, but falls off faster, Fig. 11(a). In this case the corrugation potential is smaller than the en-

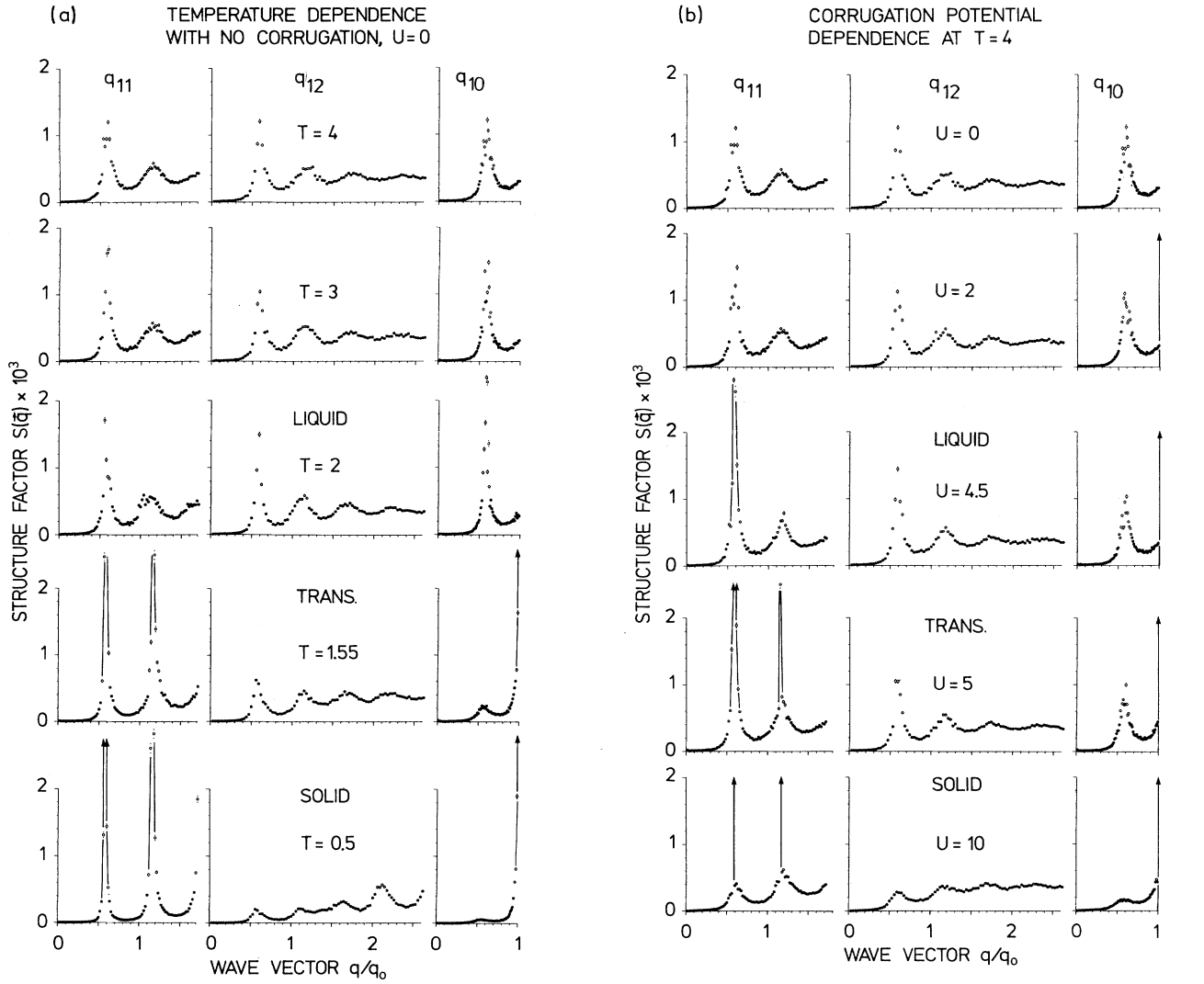

FIG. 10. (a) Sequence of structure factors for $U=0$ as a function of temperature T (heating), for three q directions: here with vector $\mathbf{q}(hk)$ corresponding to $\mathbf{q}=(h,k)q_0$. Notice the disappearence of the $\sqrt{3}\times\sqrt{3}$ Bragg peaks at $T=2$, and the isotropic liquid structure factor at high $T=4$. Examples from the solid, the transition region, and several from the liquid phase are shown. (b) Same for constant $T=4$ and as a function of the corrugation potential U (decreasing). Notice the disappearence of the Bragg peaks along the (11) direction for $U<4.5$, but the persistence of the (substrate) potential-induced (10) Bragg peak. Compare with the phase diagram, Fig. 8.

ergy corresponding to the melting temperature T_M. Notice the theory is independent of T_M, directly. It is physically reasonable that the Bragg peak is absorbed into the diffuse liquid structure factor for temperatures large relative to U and T_M. For small U the mean-square positional fluctuation around the lattice sites for the corrugation potential $\langle r^2\rangle/a^2$ is much larger close to T_M. We use the definition given in Eq. (9), $\langle r^2\rangle=\langle u^2\rangle_e+\langle r\rangle^2$. In Fig. 12 is shown the temperature variation of $\langle r^2\rangle/a^2$ for our potential for various U.

An interesting feature is that the Debye-Waller factor plot Fig. 13 shows that the peak intensity $S(\mathbf{q}_{10})$ is a universal function of the mean-square fluctuation $\langle r^2\rangle/a^2$. Figure 13 shows the same behavior irrespective of the relative values of U and T. This fact is very valuable and can be used to estimate the corrugation potential, when it is possible to calculate $\langle r^2\rangle/a^2$. An experimental determination of $S(\mathbf{q}_{10})$ as a function of T in combination with a plot like Fig. 12 allows a determination of U. The arrow at L indicates the Lindemann criterion[1] for melting in our case. The transition region in Fig. 8 falls in the range $L\leq\langle r^2\rangle/a^2\leq 0.3$.

VI. CONCLUSION

The problem of two-dimensional solids, liquids, and melting has previously been investigated in the limits of either strong or weak interaction with a supporting sub-

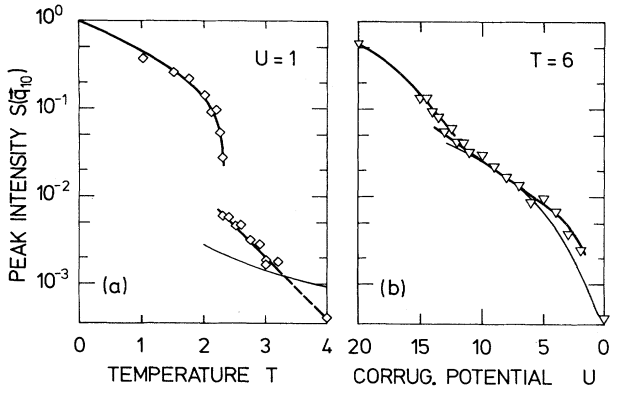

FIG. 11. (a) Peak intensity $S(\mathbf{q}_{10})$, on a logarithmic scale as a function T. Notice the linear behavior in the liquid phase, for small corrugation potential $U=1$. The line indicates the results of the linear approximation of the theory by Reiter and Moss (Ref. 21). (b) Same as a function of decreasing corrugation potential U for $T=6$.

strate and for various coverage. In this paper we have instead studied a plane in phase space spanned by temperature T and a large interval of corrugation potentials U, mainly restricting the coverage to being fixed at $\frac{1}{3}$, corresponding to a perfect $\sqrt{3}\times\sqrt{3}$ structure. The melting transition is found to occur in a monotonically increasing, relatively broad strip in the plane. The phase inside the strip, the transition region, has not been analyzed in the detail in this paper. Under the constant coverage condition used, the pressure is rapidly increasing in the transition region. This would lead to a mixed phase region at a discontinuous transition. Further studies are needed to establish the possible presence of a hexatic phase, but the different behavior of positional and orientational order parameters is not inconsistent with such a phase. The main emphasis has been laid on a investigation of the behavior of the experimentally observable

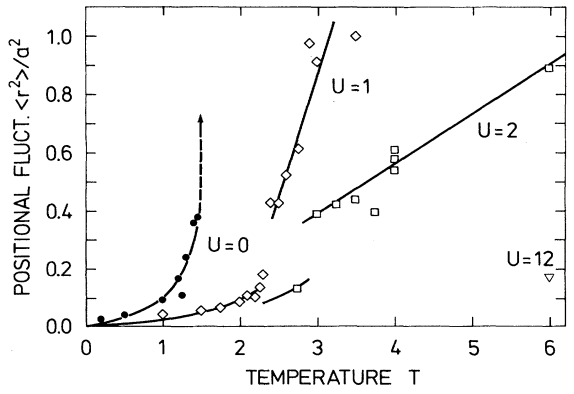

FIG. 12. The calculated positional fluctuation $\langle r^2\rangle/a^2$ for different values of U. Notice the close to linear increase with temperature for constant U and the expected dramatic increase for $U=0$. Notice also that for small $U\langle r^2\rangle/a^2$ is generally much larger near the melting point than for larger U.

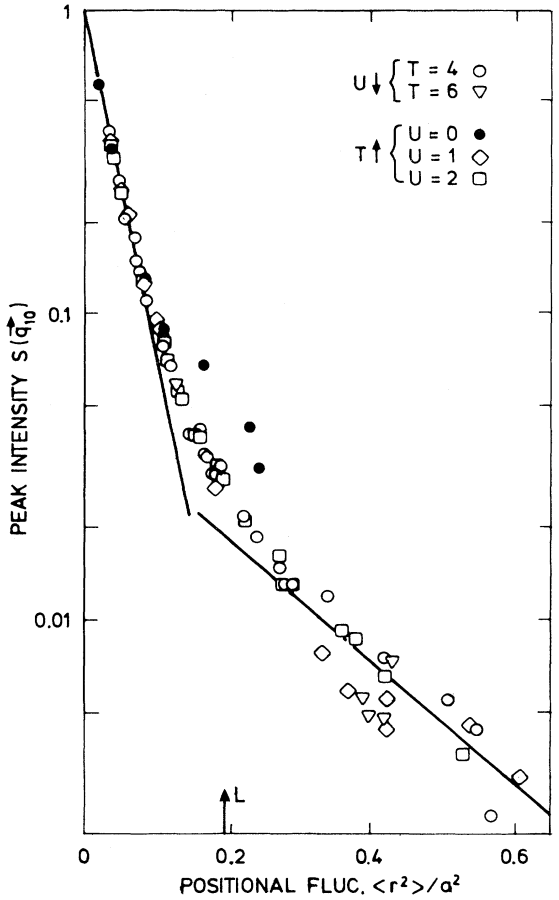

FIG. 13. A Debye-Waller plot showing that the $S(\mathbf{q}_{10})$ peak intensity is approximately a universal function of the positional fluctuation parameter $\langle r^2\rangle/a^2$ for finite corrugation potential $U\neq 0$ and for various T. It is defined in Eq. (9). The arrow at L indicates the Lindemann criterion for melting (Ref. 1). The transition region in Fig. 8 falls in the range $L\leq\langle r^2\rangle/a^2\leq 0.3$.

structure factor. It is found that the position of the first peak does not change from that of the Bragg peak position neither in the transition region nor in the liquid. If such a shift is observed it is therefore a consequence of a pressure-density variation, which of course may be indirectly coupled to the melting and the transition region. The line shape of the structure factor does not change noticeably from the transition region to well into the liquid phase. The effect of a finite corrugation potential is most clearly seen in the persistence of a Bragg peak at $\mathbf{q}=(1,0)q_0$ even in the liquid phase. This is due to the increased probability for (randomly) occupying the imaginary substrate lattice sites. As already emphasized by Reiter and Moss[21] this induced Bragg peak offers important possibilities for measuring the substrate potential U from the scattering data. We have here studied a large region of U and T. The theory[21] is a cummulant expansion and a perturbation expansion in the ratio (U/T). The linear approximation predicts a Bragg peak intensity proportional to $(U/T)^2$. This theory fits the data excel-

lently at relatively large U, close to the melting temperature T_M. For small U the fit is less satisfactory. This seems at first sight surprising. The reason is that for small U the positional fluctuations $\langle r^2 \rangle$ around the lattice sites increase rapidly above T_M. This strongly influences the determination of a Bragg peak and its peak intensity. We have found that the logarithm of the intensity decreases linearly with increasing temperature beyond the transition region. We have further found that this intensity is a universal function, for various U and T, of the mean-square displacement $\langle r^2 \rangle$ from the lattice sites. In the solid the exact Debye-Waller factor is found. In the modulated liquid another characteristic smaller factor is found. We have determined the temperature dependence of $\langle r^2 \rangle$ for some values of U and found a near linear increasing behavior in the liquid phase. Since $\langle r^2 \rangle$ is strongly dependent on U and T and is easily calculable also for other models, a valuable tool to determine U has been found.

ACKNOWLEDGMENTS

It is a pleasure to thank F. Grey and D. Vaknin for many fruitful discussions. We also thank S. C. Moss for valuable comments on the paper. E. Vives acknowledges the hospitality of the Risø National Laboratory and the Comissió Interdepartamental de Recerca i Innovació Tecnològica de la Generalitat de Catalunya for financial support.

APPENDIX A: CALCULATION OF THE STRUCUTRE FACTOR

We can consider a system with *periodic boundary conditions* as a set of $N'(N' \to \infty)$ replicas of our original $L \times L$ lattice ordered on a superlattice with lattice spacing La. This "supercell" method was used by Fan *et al.*[23] for a calculation of the anisotropic structure factor. Subsequently an interpolation between the available points were made. Let us discuss a few details of the method. The structure factor for such a system can be calculated as

$$S(\mathbf{q}) = \frac{1}{N'^2 N_p^2} \left\langle \left| \sum_{K=1}^{N'} \sum_{i=1}^{N_p} e^{i\mathbf{q}\cdot(\mathbf{X}_K + \mathbf{x}_i)} \right|^2 \right\rangle ,$$

where the first sum is a sum over the different replicas of the system, the second sum is a sum over the N_p particles on the $L \times L$ lattice, $\mathbf{X}_K$ is a vector pointing to the origin of the different replicas, and $\mathbf{x}_i$ is the position of the N_p particles inside the small lattice $L \times L$ (the unit cell). Because the superlattice structure is independent of the thermal fluctuations we can split the sum into two factors:

$$S(\mathbf{q}) = \frac{1}{N'^2} \left| \sum_{K=1}^{N'} e^{i\mathbf{q}\cdot\mathbf{X}_K} \right|^2 \frac{1}{N_p^2} \left\langle \left| \sum_{i=1}^{N_p} e^{i\mathbf{q}\cdot\mathbf{x}_i} \right|^2 \right\rangle .$$

The first term gives a set of Bragg peaks corresponding to the superlattice structure, while the second one is the structure factor of a *finite* $L \times L$ system. As a consequence the $S(\mathbf{q})$ of our system will be only different from zero on a reciprocal lattice corresponding to a triangular lattice with spacing La, and hence the resolution in the reciprocal space will depend on the direction of $\mathbf{q}$. In Fig. 1 we indicate the three directions that have been studied.

Because we have been working with $L = 90$, we can only measure 90 points along the three different segments (0,0)–(1,0), (0,0)–(2,1), and (0,0)–(1,1). This means that the resolution is higher along the (1,0) direction than along the (1,1) direction and the (2,1) direction in particular. Statistical fluctuations can be reduced by averaging over several systems of size $L \times L$. However, in order to increase the resolution it is necessary to increase the system size L. In fact one of the main reasons for using the Monte Carlo simulation, rather than molecular dynamics as in Ref. 26, is that much lager L can be studied within reasonable computer time. We have not used interpolation between points in the structure factor.

*On leave from Departament d'Estructura i Constituents de la Matèria, Facultat de Física, Universitat de Barcelona, Diagonal 647, E-08028, Spain.

[1]K. J. Strandburg, Rev. Mod. Phys. **60**, 161 (1988).
[2]N. D. Mermin, Phys. Rev. 176, 250 (1968).
[3]J. M. Kosterlitz and D. J. Thouless, J. Phys. C **6**, 1181 (1973).
[4]B. I. Halperin and D. R. Nelson, Phys. Rev. Lett. **41**, 212 (1978).
[5]P. A. Heiney, P. W. Stephens, R. J. Birgeneau, P. M. Horn, and D. E. Moncton, Phys. Rev. B **28**, 6416 (1983).
[6]E. D. Specht, M. Sutton, R. J. Birgeneau, D. E. Moncton, and P. M. Horn, Phys. Rev. B **30**, 1589 (1984).
[7]D. E. Moncton, R. Pindak, S. C. Davey, and G. S. Brown, Phys. Rev. Lett. **49**, 1865 (1982).
[8]F. F. Abraham, Phys. Rev. Lett. **44**, 463 (1980).
[9]D. Frenkel and J. P. McTague, Phys. Rev. Lett. **42**, 1632 (1979).
[10]D. S. Fisher, B. I. Halperin, and R. Mart, Phys. Rev. B **20**, 4692 (1979).
[11]R. Birgeneau and P. M. Horn, Science **232**, 329 (1986).
[12]M. S. Dresselhaus and G. Dresselhause, Adv. Phys. **30**, 139 (1981).
[13]D. A. Huse and M. E. Fisher, Phys. Rev. B **29**, 239 (1984).
[14]A. G. Naumovets, Contemporary Phys. **30**, 187 (1989).
[15]S. W. Koch and F. F. Abraham, Phys. Rev. B **27**, 2964 (1983).
[16]F. F. Abraham, Phys. Rev. Lett. **50**, 978 (1983).
[17]D. P. Di Vicenzo and E. J. Mele Phys. Rev. B **32**, 2538 (1985).
[18]A. N. Berker, S. Ostlund, and F. A. Putham, Phys. Rev. B **17**, 3650 (1978).
[19]R. G. Catlisch, A. N. Berker, and M. Kardar, Phys. Rev. B **31**, 4527 (1985).
[20]N. C. Bartelt, T. L. Einstein, and L. D. Roelofs, Phys. Rev. B **35**, 1776 (1987).
[21]G. Reiter and C. Moss, Phys. Rev. B **33**, 7209 (1986).

[22]F. Rousseaux, R. Moret, D. Guérard, P. Lagrange, and M. Lelaurian J. Phys. (Paris) Lett. **45**, L111 (1984).
[23]S. C. Moss, G. Reiter, J. L. Robertson, C. Thompson, and J. D. Fan, Phys. Rev. Lett. **57**, 3191 (1986).
[24]X. B. Kan, J. L. Robertson, S. C. Moss, K. Oshima, and C. J. Sparks, Phys. Rev. B **39**, 10 627 (1989).
[25]J. D. Fan, O. A. Karim, G. Reiter, and S. C. Moss, Phys. Rev. B **39**, 6111 (1989).
[26]E. Vives and A. Planes. Phys. Rev. A **41**, 1885 (1990).
[27]F. F. Abraham, in *Ordering in Two Dimensions,* edited by S. K. Sinha (Elsevier, Holland, 1980).
[28]O. G. Mouritsen, *Computer Studies of Phase Transitions and Critical Phenomena* (Springer-Verlag, Berlin, 1989).
[29]J. A. Barker, D. Henderson, and F. F. Abraham, Physica A **106**, 226 (1981).